PROCEEDINGS OF SCIENCE

LHC prospects for low mass ALP searches via bb final state

Amit Adhikary,[a,*] **Aoife Bharucha,**[a] **Lorenzo Feligioni**[b] **and Michele Frigerio**[c]

[a] *Aix Marseille Univ, Université de Toulon, CNRS, CPT, IPhU, Marseille, France*

[b] *Aix Marseille Univ, CNRS/IN2P3, CPPM, Marseille, France*

[c] *Laboratoire Charles Coulomb (L2C), University of Montpellier and CNRS, Montpellier, France*

E-mail: amit.adhikary@cpt.univ-mrs.fr

The current Large Hadron Collider (LHC) data does not yet show any clear indication of new physics and only incremental improvements are anticipated in the foreseeable future. However, while the main focus of the LHC has been on constraining TeV scale physics, new physics could be hiding below the electroweak scale. We consider a light axion-like particle (ALP), which could be a mediator for dark matter. If such an ALP is produced (resonantly) at the LHC it is expected to decay dominantly into the $b\bar{b}$ final state, provided its mass is $O(10-100)$ GeV. A measurement of this kind of signature is challenging due to trigger requirements at the LHC. We discuss probing these light resonances in $b\bar{b}$ final state using jet substructure techniques. We will also demonstrate strategies to improve the sensitivity by modifying trigger requirements at the LHC.

The European Physical Society Conference on High Energy Physics (EPS-HEP2025)
7-11 July 2025
Marseille, France

*Speaker

 ISSN 1824-8039 . Published by SISSA Medialab.

PoS(EPS-HEP2025)439

1. Introduction

The search for new phenomena is one of the main goals of the current and future LHC runs. Such new phenomena could come in the form of light resonances below the electroweak scale. Specifically, a light scalar or pseudoscalar, for masses above $\sim$ 10 GeV, would decay prominently to the $b\bar{b}$ final state. These spin-0 states could be well-motivated axion-like particles (ALPs) or could appear in supersymmetric models, models with an approximate R-symmetry, or composite Higgs models with additional Nambu-Goldstone bosons. In our work [1], we focus on an ALP, a that only couples to Standard Model (SM) fermions as described by the following Lagrangian:

$$\mathcal{L}_{\text{ALP}} \supset \frac{1}{2}\partial_\mu a \partial^\mu a - \frac{1}{2}m_a^2 a^2 + i\sum_f g_{\text{aff}} m_f \, a \bar{f}\gamma_5 f \,, \tag{1}$$

where m_a is the ALP mass, and g_{aff} is the ALP-fermion coupling. The ALP mass is chosen in the range from 10 GeV to 100 GeV. Our objective is to devise an optimised analysis strategy which would results in an improved sensitivity to the $b\bar{b}$ final state at the HL-HLC. This strategy would involve triggering on a high-p_{T} photon, recoiling against a large-radius jet of a collimated $b\bar{b}$ pair. We further show that the sensitivity can be improved by considering modified trigger requirements. We also compare our bounds with the existing ones in the ALP parameter space, defined by the plane m_a-g_{aff}.

2. Collider Analysis

The signal process consists of an ALP produced with a back-to-back high p_{T} isolated photon. Thus the ALP is boosted and the decay products, $b\bar{b}$, can be accommodated in a large radius jet with two-prong jet substructure. Multijet production along with a photon is the main source of SM background in this channel, while a subdominant contribution arises from $W + \gamma$ and $Z + \gamma$ processes. The signal and background processes are generated using `MadGraph5_aMC@NLO` [2] and `Pythia8` [3], respectively. The showering and hadronisation are performed with `Pythia8`. The detector effects are simulated with `Delphes-3.5.0` [4]. Here we use the default HL-LHC ATLAS analysis card. The collider analysis involves several steps. First, we construct a large radius jet with hadronisation objects from the bottom pairs in the final state. Next, we utilise prong discriminant observable constructed using the large radius jet, to significantly reduce the backgrounds. We also apply double b-tagging algorithm to improve signal sensitivity. Finally, we calculate the signal and background events by selecting a region in the large radius jet mass distribution.

The large radius jet is reconstructed using the `FastJet` framework [5]. We utilise the AK1.0 anti-k_{T} clustering algorithm that uses particle-flow objects in Delphes. The trigger requirements on the associated photon are $p_{\text{T},\gamma} > 160$ GeV and $|\eta_\gamma| < 2.1$ [6]. In the $\eta - \phi$ plane, the photon is separated from the AK1.0 jet by $\Delta R > 2.2$. We further apply soft drop mass algorithm [7] to remove soft wide angle radiation from the AK1.0 jet, using the parameters $z_{cut} = 0.1$ and $\beta = 1$ [8] where, z_{cut} and β are the energy threshold and angular exponent required to satisfy the soft drop condition. The invariant mass of the soft dropped AK1.0 jet is referred as m_{SD}. Next, we use the designed decorrelated tagger (DDT) [9] observable N_2^{DDT}, to distinguish the AK1.0 jet between a clear 2-prong substructure of bottom pair from ALP decay and one prong substructure for multijet

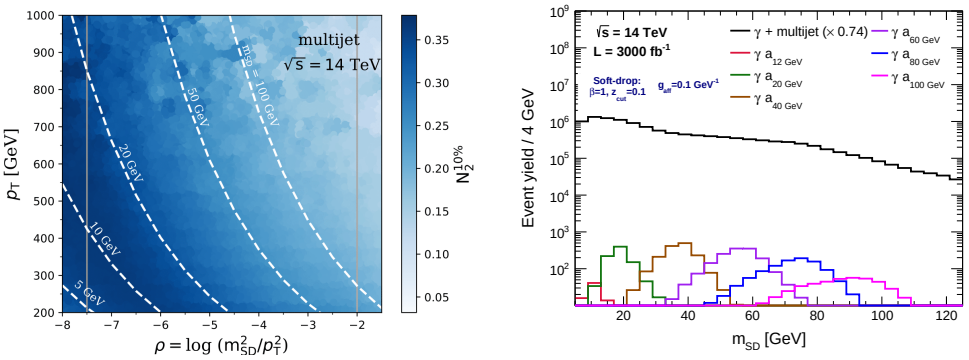

Figure 1: (left) The $N_2^{10\%}$ values in the $\rho - p_T$ plane for multijet background. (right) The soft drop mass distributions of AK1.0 jet for the multijet background and ALP signal.

background. It is defined as, $N_2^{DDT}(\rho, p_T) \equiv N_2 - N_2^{10\%}(\rho, p_T)$. Here, N_2 is a 2-prong discriminant variable. $N_2^{10\%}$ corresponds to the value of N_2 that keeps 10% of the multijet backgrounds. This depends on the jet transverse momentum and a scaling variable, ρ, as illustrated in Fig. 1 (left). We choose $-7.5 \leq \rho \leq -2.0$ to efficiently select the signal in the m_{SD} range from 5 GeV to 100 GeV. The requirement of $N_2^{DDT} < 0$, by definition, selects 10% of multijet background. However, the signal efficiency is between $\sim$ 12% and 26%. That increases the signal over background ratio. The only exception being the highly collimated ALP case for $m_a = 12$ GeV with efficiency around 1%, where the 2-prong feature is lost. The m_{SD} distribution for the signal and multijet background is illustrated in Fig. 1 (right). The shape of the solid black line for multijet background agrees well with Ref. [6, 10], upon applying a data-Monte Carlo scale factor of 0.74 [10].

The ALP signal contains b-quarks in the final state. Thus the signal sensitivity can be improved by applying the b-tagging algorithm. We apply double b-tagging algorithm [11] outside the detector simulation tool, `Delphes`. It is basically a flavor dependent parametrisation of bb tagging probabilities, multiplied by a working point of 80% bb tagging efficiency and corresponding rejection efficiencies for multijet background based on GN2X performance [11]. The idea behind parametrisation is to identify smaller radius jets, called subjets, inside the AK1.0 jet and match them to a hadron in the event. It classifies the AK1.0 jet into different double flavour jets. To reconstruct the subjets, we utilise the variable radius (VR) anti-k_T jets [12]. The advantage of using VR algorithm is that it can identify the substructure coming from a hard parton than from soft radiation. The radius of the VR jet changes according to the jet transverse momentum, $R_{\text{eff}}(p_T) = \rho_{VR}/p_T$, where ρ_{VR} is a dimensionful constant. We optimise ρ_{VR} for the chosen ALP masses in order to maximise the double subjet b-labelling efficiency [12]. Next, we match the VR subjets to a hadron following the recipe in Ref. [13]. The signal AK1.0 jet is chosen with at least two VR subjets labelled as b-jets (bb). For the multijet background, the two flavor matched VR subjets can have the following flavour compositions: bb, bc, bl, cc, cl, and ll. The final task is to count the number of signal and background events. We estimate it by considering a mass window around the reconstructed ALP mass, m_{SD}. The resolution of m_{SD} distribution for each ALP mass is calculated using a double-sided Crystal Ball function [14] that performs better under the shape change of ALP resonance peak. Thus the core of the m_{SD} distribution is fitted by a Gaussian function while using

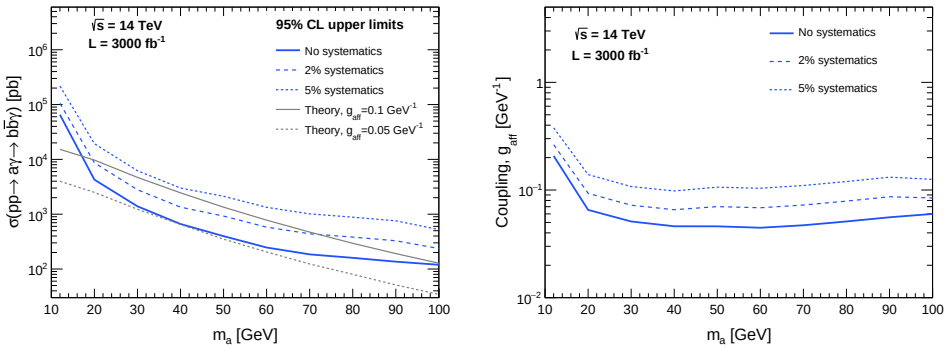

Figure 2: Upper limit at 95% C.L. on $\sigma(pp \to a\gamma \to b\bar{b}\gamma)$ on the left panel and ALP-fermion coupling g_{aff} on the right panel, as a function of the ALP mass at $\sqrt{s} = 14$ TeV with $\mathcal{L} = 3000$ fb^{-1}.

a power law function on both sides of the distribution. For each ALP mass, we choose the mass window in the range of $[\mu - \sigma, \mu + \sigma]$, where μ and σ are the mean value and width of the fitted Gaussian part of the Crystal Ball distribution. As mentioned earlier, the signal efficiency is low at $m_a = 12$ GeV as the 2-prong substructure is absent for such highly boosted ALP. The fitted width, σ increases for heavier ALPs because the decay products are less collimated and may fall outside the AK1.0 jet cone.

3. Results

The results are presented in terms of upper exclusion limits on the production cross-section of $b\bar{b}\gamma$ process and the ALP-fermion coupling, g_{aff}, at 95% confidence level (CL). For the signal significance we use, $S/\sqrt{N_{\text{B}}} > N_{\text{CL}}$, where $N_{\text{CL}} = 2$ corresponds to 95% CL. The signal yield is calculated with $S = \sigma(pp \to a\gamma \to b\bar{b}\gamma) \cdot \epsilon \cdot \mathcal{L}$ where $\sigma(pp \to a\gamma \to b\bar{b}\gamma)$ is the signal production cross-section, ϵ is the signal efficiency after the analysis, and $\mathcal{L}$ corresponds to the integrated luminosity. The 95% CL upper limit on $\sigma(pp \to a\gamma \to b\bar{b}\gamma)$ as a function of the ALP mass is shown in Fig. 2(left), at $\sqrt{s} = 14$ TeV and $\mathcal{L} = 3000$ fb^{-1}. The solid, dashed and dotted blue line correspond to the exclusion limits with null, 2% and 5% systematic uncertainty, respectively. The upper limits on $\sigma(pp \to a\gamma \to b\bar{b}\gamma)$ vary between $6.5 \cdot 10^4$ pb and 119 pb for $m_a = 12$ GeV and 100 GeV, with null systematics. The cross-section exclusion limits are translated into the upper limits on g_{aff} and are shown in Fig. 2(right). The limit is stronger for $m_a \simeq 60$ GeV, $g_{\text{aff}} \leq 0.045$ GeV^{-1}, but weakens in the range $m_a \sim (70 - 100)$ GeV, $g_{\text{aff}} \lesssim (0.047$ - $0.060)$ GeV^{-1}.

We further explore the case of lowering the p_{T} threshold on the recoiling photon from $p_{\text{T},\gamma} > 160$ GeV to 100 GeV. The motive is to assess any possible improvement on the ALP signal sensitivity in the low mass regime. We repeat the collider analysis with $p_{\text{T,AK1.0}} = 100$ GeV. The upper limits on both the cross-section $\sigma(pp \to a\gamma \to b\bar{b}\gamma)$ and ALP-fermion coupling g_{aff} improve below $m_a \simeq 70$ GeV. The cross-section limits improve by a factor four at $m_a = 12$ GeV. A maximal sensitivity for ALP-fermion coupling is obtained around $m_a = 30 - 40$ GeV with $g_{\text{aff}} \simeq 0.023$ GeV^{-1}. Therefore, lowering the p_{T} threshold requirement for the recoiling photon improves the sensitivity to low-mass ALP searches.

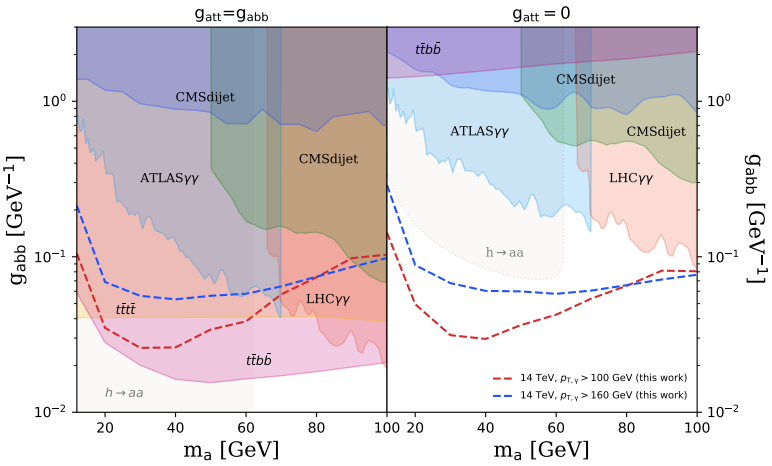

Figure 3: The collider constraints along with our derived bounds in the plane of $m_a - g_{\rm aff}$. On the left panel, the constraints include the ALP couplings to top and bottom quark, while the ALP only couples to bottom quark for the bounds shown on the right panel.

Finally in Fig. 3, the results are interpreted in the ALP parameter space, defined by the m_a - $g_{\rm aff}$ plane, along with the existing collider constraints. Importantly, these constraints greatly rely on the ALP-top quark coupling that has little relevance for our ALP signal. We therefore show two cases: $g_{\rm att} = g_{\rm abb}$ on the left panel and $g_{\rm att} = 0$ on the right panel, of Fig. 3. Our derived projected limits are shown by the blue and red dashed lines for $p_{\rm T,\gamma} > 160$ GeV and $p_{\rm T,\gamma} > 100$ GeV, respectively. In the left panel where ALP couples to both the up-type and down-type quarks, the $t\bar{t}b\bar{b}$ search excludes a larger region than that from $\gamma + b\bar{b}$ derived in this work. The flat yellow bound is from $t\bar{t}t\bar{t}$ process and weaker than the $\gamma + b\bar{b}$ sensitivity for $p_{\rm T,\gamma} > 100$ GeV, in the range $m_a \sim$ 20-60 GeV. The constraint from di-photon searches is weaker than the $\gamma + b\bar{b}$ bounds below $m_a \sim$ 65 GeV. Similarly, the bounds from di-jet searches are weaker than those we obtain. The dotted line and pale-gray shaded region corresponds to constraints from $\mathbf{h} \to$ BSM bound. For this, we evaluate the $h \to aa$ branching ratio because it is the dominant BSM decay channel of the Higgs boson in the ALP model. However, this constraint can be relaxed by a cancellation between loop contributions from heavy quark (mainly top) and tree-level contributions from dim-6 operator such as $(\partial_\mu a)(\partial_\mu a)H^\dagger H$. The constraints on the right panel of Fig. 3 correspond to setting $g_{\rm att} = 0$, where the ALPs interact dominantly with down-type quarks. In this scenario, our projected bounds from $\gamma + b\bar{b}$ are stronger than the existing collider constraints. For example, the $t\bar{t}b\bar{b}$ bound comes from quark-initiated diagrams that include top-quark emission from SM gauge or Higgs bosons. The processes $h \to aa$ and $a \to \gamma\gamma$ contain only the bottom quark loop contribution. The $t\bar{t}t\bar{t}$ production vanishes for $g_{\rm att} = 0$. In comparison, our derived upper bound on $g_{\rm abb}$ is roughly scaled by a factor of $\sqrt{2}$.

4. Summary and outlook

The search for light resonances is an important probe to understand physics beyond the SM. We specifically considered a light pseudoscalar ALP decaying via the $b\bar{b}$ final state, in the mass

range of 10 GeV to 100 GeV. We increased the analysis sensitivity to light ALPs by demanding a high p_T photon recoiling against the ALP. Since the ALP is boosted, we used jet substructure techniques to reconstruct the ALP decay products. QCD multijet production is the dominant background contribution in this channel. We carefully matched our Monte Carlo simulation of multijet production with available data-driven techniques. We utilised a two prong discriminant observable, N_2, to separate the signal two-prong substructures from the one prong structure of multijet background. An important part of the analysis involves the $b\bar{b}$-tagging of the AK1.0 jet, to further improve the signal efficiency. We applied this technique outside the detector simulation software, but an automatic implementation in `Delphes` might be useful for future works. The obtained exclusion limits on the $b\bar{b}\gamma$ production cross-section provide significantly better results as compared to existing LHC searches at the current run. In case the trigger requirements on the photon p_T can be reduced further by the ATLAS and CMS collaboration, our study shows that the sensitivity to low mass scenarios can be enhanced. The ALP parameter space is also explored, where collider searches are the main source of constraints in the considered mass range for the ALPs. Stronger constraints than ours come from the $t\bar{t}b\bar{b}$ searches. However, in models with dominant ALP coupling to down-type quarks, our analysis provides the most powerful direct search constraint for the ALP. The analysis strategy proposed here can be easily applied to any well-motivated low-mass resonance search via the $b\bar{b}$ final state.

References

[1] A. Adhikary, A. Bharucha, L. Feligioni and M. Frigerio, *Prospects for sub-EW-scale ALP searches via γ+bb¯ signatures at the LHC using jet substructure techniques*, *Phys. Rev. D* **112** (2025) 055042 [2410.09033].

[2] J. Alwall, R. Frederix, S. Frixione, V. Hirschi, F. Maltoni, O. Mattelaer et al., *The automated computation of tree-level and next-to-leading order differential cross sections, and their matching to parton shower simulations*, *JHEP* **07** (2014) 079 [1405.0301].

[3] T. Sjöstrand, S. Ask, J.R. Christiansen, R. Corke, N. Desai, P. Ilten et al., *An introduction to PYTHIA 8.2*, *Comput. Phys. Commun.* **191** (2015) 159 [1410.3012].

[4] DELPHES 3 collaboration, *DELPHES 3, A modular framework for fast simulation of a generic collider experiment*, *JHEP* **02** (2014) 057 [1307.6346].

[5] M. Cacciari, G.P. Salam and G. Soyez, *FastJet User Manual*, *Eur. Phys. J. C* **72** (2012) 1896 [1111.6097].

[6] CMS collaboration, *Search for Low-Mass Quark-Antiquark Resonances Produced in Association with a Photon at $\sqrt{s}$ =13 TeV*, *Phys. Rev. Lett.* **123** (2019) 231803 [1905.10331].

[7] A.J. Larkoski, S. Marzani, G. Soyez and J. Thaler, *Soft Drop*, *JHEP* **05** (2014) 146 [1402.2657].

[8] ATLAS collaboration, *Identification of hadronically-decaying top quarks using UFO jets with ATLAS in Run 2*, Tech. Rep. ATL-PHYS-PUB-2021-028, CERN, Geneva (2021).

[9] J. Dolen, P. Harris, S. Marzani, S. Rappoccio and N. Tran, *Thinking outside the ROCs: Designing Decorrelated Taggers (DDT) for jet substructure*, *JHEP* **05** (2016) 156 [1603.00027].

[10] CMS collaboration, *Search for low mass vector resonances decaying into quark-antiquark pairs in proton-proton collisions at* $\sqrt{s} = 13$ *TeV*, *JHEP* **01** (2018) 097 [1710.00159].

[11] ATLAS collaboration, *Transformer Neural Networks for Identifying Boosted Higgs Bosons decaying into* $b\bar{b}$ *and* $c\bar{c}$ *in ATLAS*, Tech. Rep. ATL-PHYS-PUB-2023-021, CERN, Geneva (2023).

[12] ATLAS collaboration, *Variable Radius, Exclusive-*k_T*, and Center-of-Mass Subjet Reconstruction for Higgs(*$\to b\bar{b}$*) Tagging in ATLAS*, Tech. Rep. ATL-PHYS-PUB-2017-010, CERN, Geneva (2017).

[13] ATLAS collaboration, *Identification of Boosted Higgs Bosons Decaying Into* $b\bar{b}$ *With Neural Networks and Variable Radius Subjets in ATLAS*, Tech. Rep. ATL-PHYS-PUB-2020-019, CERN, Geneva (2020).

[14] *Search for scalar diphoton resonances in the mass range 65-600 GeV with the ATLAS detector in pp collision data at* $\sqrt{s} = 8$ *TeV*, Tech. Rep. ATLAS-CONF-2014-031, CERN, Geneva (2014).

PoS(EPS-HEP2025)439